



## Characterizing dissolved organic matter fouling of nanofiltration membranes and evaluating effects of naproxen retention

Guizhen Feng<sup>a,b</sup>, Huaqiang Chu<sup>a,\*</sup>, Bingzhi Dong<sup>a,\*</sup>

<sup>a</sup>State Key Laboratory of Pollution Control and Resource Reuse, Key Laboratory of Yangtze River Water Environment, Ministry of Education, School of Environmental Science and Engineering, Tongji University, Shanghai 200092, China, Tel./Fax: +86 21 65982691; email: fgz77@sina.com (G. Feng), Tel./Fax: +86 21 65985811; email: huaqiang\_chu@163.com (H. Chu), Tel./Fax: +86 21 65982691; email: dbz77@tongji.edu.cn (B. Dong)

<sup>b</sup>School of Civil Engineering and Architecture, East China Jiaotong University, Jiangxi 330013, China

Received 11 March 2014; Accepted 5 September 2014

---

### ABSTRACT

Nanofiltration (NF) membrane fouling caused by two types of natural dissolved organic matter (DOM), namely Qingcaosha reservoir (QCS) DOM and Taihu Lake (TH) DOM, on naproxen (NPX) retention, were assessed. The results indicated that NPX retention could be interpreted with respect to the DOM molecular weights (MW) and the fouling characteristics. Organics with medium- and low-MW, e.g. less than 10 kDa, significantly affected NPX retention and resulted in membrane fouling. DOMs with medium MW (1.5–10 kDa) mainly had strong hydrophobic characteristics, and adhered well to the NF membrane surface to form a fouling layer, which altered the hydrophobicity and negative charge of the membrane surface. The hydrophobicity and electronegativity of the adhered DOM fouling layer was responsible for the decreased membrane flux and the change in NPX retention. TH DOM contained more hydrophobic organics with MW 1.5–10 kDa than QCS DOM, and the cohesion free energy and adhesion free energy between the membrane and foulants were more negative for TH DOM, which caused more severe membrane fouling. The surface free energy between membranes and foulants is a useful parameter for membrane fouling analysis, and a mechanism of influencing NPX retention in the presence of DOM was proposed. The increased NPX removal by QCS DOM-fouled membrane was mainly attributed to electrostatic repulsion, whereas the decreased NPX rejection by TH DOM-fouled membrane was mainly attributed to cake-enhanced concentration polarization.

*Keywords:* Dissolved organic matter; Membrane fouling; Naproxen; Nanofiltration; Removal efficiency

---

### 1. Introduction

Membrane separation, a new and highly efficient separation technology, has great potential for applications in water treatment [1,2]. The removal of

micropollutants has gradually aroused extensive concern, and nanofiltration (NF) and other high-pressure membrane filtration processes have been shown to provide viable barriers against a wide range of micropollutants [3–6]. Membrane fouling is the most important problem encountered in drinking-water membrane filtration treatment [7,8]. In natural water

---

\*Corresponding authors.

resources, dissolved organic matter (DOMs) include all organic matter filtered through a 0.45- $\mu\text{m}$  membrane such as colloids and polysaccharides, proteins, humic acids, and fatty acids [9–11]. Previous studies have shown that the presence of DOM has a great influence on the decrease in membrane flux, and results irreversible membrane fouling [12,13]. The DOMs in natural waters from different origins differ greatly in composition, type, molecular weight (MW), and chemical properties such as pH, ionic strength, and heavy-metal content [14]. Consequently, the induced degrees of membrane fouling and the fouling mechanisms are different. Many studies have shown that the presence of DOM greatly influences the fate and behavior of micropollutants and their removal by NF membranes, and differences among the results have been attributed to the different types of micropollutants used and to the complexities of the retention mechanisms [15–18]. However, the effect of membrane fouling on the mechanisms of micropollutant rejection, such as hydrophobic adsorption and electrostatic repulsion, remains poorly understood.

Many studies of membrane fouling have been conducted in general laboratories by adding representative standard materials to raw water to investigate the membrane-fouling process. Nghiem et al. [19] investigated the fouling of NF membranes by humic acids, using bisphenol A (BPA) as an indicator, to identify the various mechanisms that may lead to changes in solute rejection. The results of this study showed that pore blocking and cake-enhanced membrane fouling influenced BPA rejection, and the relative contribution of these processes was largely dependent on the membrane pore size. In their subsequent research [20], humic acids, alginate, bovine serum albumin, and silica colloids were selected as model foulants, and the authors reported that the influence of membrane fouling on the retention of trace organic contaminants was governed by four distinct mechanisms: modification of the membrane charge surface, pore blocking, cake-enhanced concentration polarization, and modification of the membrane hydrophobicity. This approach is excellent for studying the mechanism of membrane fouling, but provides little information on membrane fouling caused by organic matter in natural waters. The use of natural waters in membrane-fouling research has great practical significance. Naproxen (NPX) is an anti-inflammatory, antipyretic, and analgesic nonsteroidal drug, and is a typical example of pharmaceuticals and personal care products. NPX has been detected as a trace pollutant in water environments [21–23], and recent studies have shown that long-term intake of NPX trace levels not only

contributes to heart disease and stroke but can also cause pulmonary toxicity [24].

The aim of this study was to investigate the effects of membrane fouling caused by different natural DOM on NPX removal using NF membranes, and to understand NF membrane fouling in the presence of DOM in terms of the interaction between NPX and the membrane surface. Two commercially available NF membranes with different characteristics were selected for this investigation, and the mechanisms that could account for the effects of membrane fouling on NPX rejection were systematically investigated and described.

## 2. Materials and methods

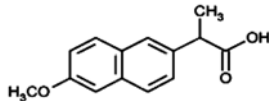
### 2.1. Materials

The NPX solution was obtained by dissolving a certain amount of NPX in Milli-Q water. The main physicochemical properties of NPX (HPLC-grade, Sigma–Aldrich) are presented in Table 1.

The fouling experiments were carried out using two different natural sources of DOMs, namely water from Taihu Lake (TH; Jiangsu Province, China) and from the Qingcaosha reservoir (QCS; Shanghai, China) (Table 2). The raw water samples obtained from the natural environments were concentrated by a reverse-osmosis to approximately 10 mg/L total organic carbon (TOC), determined using a TOC analyzer (TOC-V<sub>CPH</sub>, Shimadzu). The water samples were then filtered through a Millipore 0.45  $\mu\text{m}$  filter. The calcium ion concentration of the raw waters was adjusted to 1 mmol/L in the experiments [19]. The pH value was adjusted to 8.0 using 1 mol/L HCl and 1 mol/L NaOH.

The NF membranes (HL and ESNA1-K) (Table 3), which were supplied by GE-Osmonics and Hydranautics, respectively, were polyamide thin-film composites

Table 1  
Physicochemical properties of NPX

| Items                                       | Values  |
|---|---|
| CAS number                                  | 22204-53-1  |
| The molecular formula                       | C <sub>14</sub> H <sub>4</sub> O <sub>3</sub>   |
| Molecular weight                            | 230.2   |
| Solubility (water, 25°C)/mg L <sup>a</sup>  | 25.0  |
| log <i>K</i> <sub>OW</sub> <sup>a</sup>     | 3.18  |
| p <i>K</i> <sub>a</sub> (20°C) <sup>a</sup> | 4.2   |
| Molecular structure                         |  |

<sup>a</sup>Experimental database: SRC PhysProp database.

Table 2  
Water quality of source waters

| Raw water | Turbidity (NTU) | pH   | DOC (mg/L) | UV <sub>254</sub> (cm <sup>-1</sup> ) | SUVA (L/mg m) |
|-----------|-----------------|------|------------|---------------------------------------|---------------|
| QCS       | 4.69            | 8.01 | 3.27       | 0.039                                 | 1.16          |
| TH        | 34.80           | 8.57 | 4.56       | 0.087                                 | 1.91          |

Table 3  
Characteristics of the membranes

| Membrane               | MWCO <sup>a</sup><br>(Da) | Material      | Roughness <sup>b</sup><br>(nm) | Contact<br>angle (°) | Pure water<br>permeability <sup>c</sup><br>(L/d m <sup>2</sup> kPa) |
|------------------------|---------------------------|---------------|--------------------------------|----------------------|---|
| HL (GE-Osmonics)       | 380                       | Polyamide TFC | 5.876                          | 35.9                 | 3.6   |
| ESNA1-K (Hydranautics) | 380                       | Polyamide TFC | 55.076                         | 60.7                 | 1.3   |

<sup>a</sup>Material and MW cut-off (MWCO) information were obtained from the manufacturer.

<sup>b</sup>Average roughness values were measured in tapping mode with a scan size 10 μm × 10 μm by AFM (Nano Scope IV, VEECO, USA).

<sup>c</sup>Values were measured with Milli-Q water at 20°C and 500 kPa.

with a microporous polysulfone supporting layer. The virgin membranes were presoaked in Milli-Q water for over 48 h to remove humectants.

## 2.2. Membrane fouling and NPX retention experimental protocols

A crossflow membrane filtration test unit (SEPA CF II, GE Osmonics) was used in this study (Fig. 1) which had an effective membrane area of 140 cm<sup>2</sup>. Both the permeate and the concentrate were recycled to the feed tank except for the samples withdrawn for analysis. The recovery ( $Q_{\text{permeate}}/Q_{\text{feed}}$ ) was set at approximately 10% under a constant operating pressure of 450 kPa. The permeate flow rate was measured using a digital flow-meter (5013L, Smith) connected to

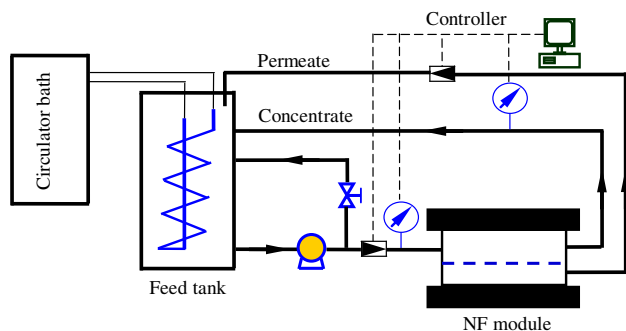


Fig. 1. Schematic diagram of the NF filtration test unit.

a PC. The temperature of the feed water was kept constant at 20°C using a temperature controller (Haake SC100-A10, Thermo Fisher Scientific).

The fouling and subsequent retention experimental protocol consisted of three steps: compacting, fouling development, and retention tests. First, the membrane was compacted using deionized water at 800 kPa for at least 1 h until a stable baseline flux was achieved. The fouling layer was then allowed to develop, using feed waters containing natural DOM, at concentrations of approximately 10 mg/L TOC. The volume of the feed water solution was 5 L. This fouling development step was carried out for 8 h and the feed water was maintained at pH 8.0. After development of the organic fouling layer, the feed reservoir was spiked with the appropriate amount of NPX solution to obtain a concentration of 100 μg/L. The solution pH was maintained at 8.0, and the filtration time was 8 h. To examine NPX retention by the clean membranes, a similar protocol without the fouling development step, was used.

## 2.3. Analytical methods

### 2.3.1. Chemical analysis

The detection and quantification of NPX were performed using a high-performance liquid chromatography (HPLC; Agilent 1200, USA). The HPLC system was equipped with an ultraviolet (UV) detector (240 nm) and a Waters XBridge<sup>TM</sup> C18 reversed phase

column (4.6 mm × 150 mm). A methanol/water (70:30) solution containing 0.1% acetic acid was used as the eluent at a flow rate of 0.7 mL/min and column temperature of 35°C. The sample injection volume was 50 µL and the test time was 7 min. In the range of experimental concentrations used, a linear calibration curve was obtained with a coefficient of determination ( $R^2$ ) of 0.9999. The detection limit of NPX using this method was approximately 1 µg/L.

### 2.3.2. NPX rejection and membrane flux

The NPX rejection ( $R$ ) and membrane flux ( $J$ ) were calculated using the following equations:

$$R = \frac{C_f - C_p}{C_f} \times 100\% \quad (1)$$

$$J = \frac{Q}{A \cdot t} \quad (2)$$

where  $C_f$  and  $C_p$  are the concentrations of the feed and permeate (µg/L), respectively,  $Q$  is the permeate volume (L),  $A$  is the membrane area (m<sup>2</sup>),  $t$  is the filtration time (min), and  $J$  is the filtration flux of the membrane [L/(m<sup>2</sup> h)]. The experimental flux was calculated using the ratios of filtration flux  $J$  to the initial flux  $J_0$  ( $J/J_0$ ) in order to compare the membrane-fouling potentials.

### 2.3.3. MW distribution

The MW distributions of the samples were determined using high-performance size-exclusion chromatography-UV/visible detection-total organic carbon analysis (HPSEC-UV-TOC). HPSEC was performed using a TSK G3000 SW<sub>xl</sub> (Tosoh) column (2 mm × 250 mm). The HPLC system (e2650, Waters) was equipped with a UV detector (2489 UV detector, Waters) operated at 254 nm, and an on-line TOC detector (Sievers Total Organic Carbon Analyzer 900 Turbo, GE).

Amberlite XAD-8, XAD-4 and IRA-958 were used to separate the DOM into hydrophobic and hydrophilic fractions [25]. The MW distribution of each fraction was determined.

### 2.3.4. Characterization of fouled membrane

Contact angle measurements were performed with a contact-angle-measuring instrument (DCA15, Germany), using the standard sessile drop method.

Milli-Q water was used as the reference liquid. The fouled membranes were air dried prior to the measurements. The average value of the right and left contact angles was used in this work. The measurement time was limited to 6 s to avoid water adsorption by the membrane. Measurements were conducted on each sample at least seven times to ensure experimental accuracy, and the average value of the contact angle was reported.

Scanning electron microscopy (SEM) was used to examine the top surface and a cross section of the membranes; the samples were gold sputtered, and then examined using a Tescan instrument (Czech Republic). Atomic force microscopy (AFM) was used to analyze the surface morphology and roughness of the membranes. Small squares of the membranes (approximately 1 cm<sup>2</sup>) were cut and glued on a glass substrate. The membrane surface was then imaged over a scan area of 5 µm × 5 µm using a NanoScope VI instrument (Veeco) in tapping mode.

Attenuated total reflectance Fourier-transform infrared (FTIR) spectroscopy was used to provide insights into the chemical nature of the deposits on the NF membranes. The FTIR spectra of the fouled membranes were recorded using a Spotlight 400 spectrometer (Perkin-Elmer, USA). The average number of scans was 32, and the range recorded was 600–4,000 cm<sup>-1</sup>.

### 2.3.5. Calculation of surface free energy

The surface free energy can be calculated from the surface tension and zeta potential. Based on DLVO theory, the total interaction energy between a solute and membrane can be accounted for by the Lifshitz-van der Waals force (LW) and the electrostatic force (EL) interaction energies, as shown in Eq. (3). There is also an important acid–base (AB) interaction energy, including electron-donating ( $\gamma^-$ ) and electron-accepting ( $\gamma^+$ ) terms, between the membrane and solute in aqueous systems [26]. Therefore, the DLVO approach was used to evaluate the total interaction energy ( $\Delta G^{\text{TOT}}$ ) between the membrane and the solute (Eq. (4)) [24,26].

$$\Delta G^{\text{TOT}} = \Delta G^{\text{LW}} + \Delta G^{\text{EL}} \quad (3)$$

$$\Delta G^{\text{TOT}} = \Delta G^{\text{LW}} + \Delta G^{\text{AB}} + \Delta G^{\text{EL}} \quad (4)$$

The LW is the attraction energy for both solution–solution and solution–membrane interactions in an aqueous environment; Eq. (5) is a simplified equation, which estimates the LW interaction between the solution and the membrane [26]. The subscripts f, w, and

m represent the foulant, water, and membrane, respectively.

$$\Delta G_{fwm}^{LW} = \left( \sqrt{\gamma_w^{LW}} - \sqrt{\gamma_m^{LW}} \right) \left( \sqrt{\gamma_f^{LW}} - \sqrt{\gamma_w^{LW}} \right) \quad (5)$$

The EL can be either repulsive or attractive for both foulant–foulant and foulant–membrane interactions in an aqueous environment, and the simplified equation for the determination of the EL interaction between the foulant and the membrane is shown in Eq. (6) [26].

$$\Delta G_{fwm}^{EL} = \frac{\epsilon_r \epsilon_0 \kappa}{2} \times (\zeta_f^2 + \zeta_m^2) \times [1 - \coth(\kappa y) + (2\zeta_f \zeta_m) \times \frac{\text{csch}(\kappa y^0)}{\zeta_f^2 + \zeta_m^2}] \quad (6)$$

where  $\epsilon_0, \epsilon_r$  is the dielectric permittivity of the fluid,  $\zeta_f$  and  $\zeta_m$  represent the surface potentials of the foulant and membrane, respectively,  $\kappa$  is the inverse Debye screening length, and  $y^0$  is the minimum equilibrium cut-off distance (0.157 nm ± 0.009 nm) [26].

In a polar system, the AB interaction between the foulant and membrane is given by Eq. (7) [26].

$$\Delta G_{fwm}^{AB} = 2\sqrt{\gamma_w^+} \left( \sqrt{\gamma_m^-} + \sqrt{\gamma_f^-} - \sqrt{\gamma_w^-} \right) + 2\sqrt{\gamma_w^-} \left( \sqrt{\gamma_m^+} + \sqrt{\gamma_f^+} - \sqrt{\gamma_w^+} \right) - 2 \left( \sqrt{\gamma_f^- \gamma_m^+} + \sqrt{\gamma_f^+ \gamma_m^-} \right) \quad (7)$$

Previous studies [27] have suggested that the contribution of the EL force energy is very small compared with the other surface energy components; therefore, we disregarded the EL contribution and used the LW and AB interactions to analyze the influence of DOM on membrane fouling, as shown in Eq. (8).

$$\Delta G^{TOT} = \Delta G^{LW} + \Delta G^{AB} \quad (8)$$

### 3. Results and discussion

#### 3.1. Flux decline behaviors of different membranes with different DOMs

Fig. 2 shows the membrane permeate fluxes during fouling development. Severe membrane fouling can be observed in the presence of DOM. The formation of a fouling layer was visually confirmed at the end of

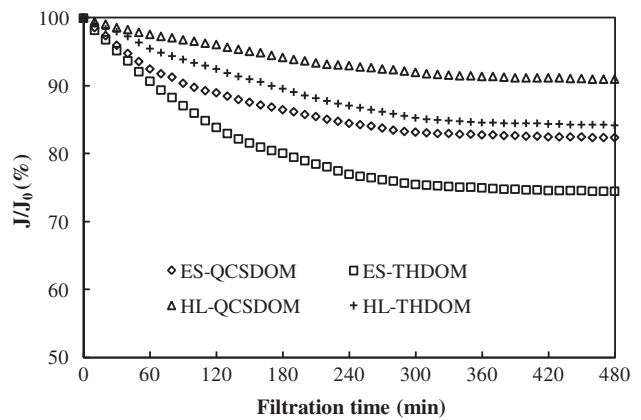


Fig. 2. Membrane flux decline behaviors during 8 h of NF in the presence of DOM.

Note: The legend “ES” represent the ESNA1-K membrane.

each experiment, and a fouling layer of organics firmly attached to the membrane surface was observed.

Fig. 2 indicates that the presence of DOM resulted in a decline in filtration flux, which was related to the type of DOM. The decline in filtration flux caused by membrane fouling can be expressed as  $J/J_0$ : lower values of  $J/J_0$ , indicate a greater decline in filtration flux and more severe membrane fouling. During membrane-fouling development, the value of  $J/J_0$  associated with TH DOM was lower than that of QCS DOM for both the NF membranes, which suggested that TH DOM caused more severe membrane fouling than QCS DOM. Fig. 2 also shows that the membrane flux attenuations of the different NF membranes were different in the presence of the same type of DOM. Compared with the HL membrane, the ESNA1-K membrane exhibited a faster decrease in membrane flux with the normalized flux reduced to 82.4% for QCS DOM and 74.5% for TH DOM at the end of the filtration stages. This result indicated that membrane fouling of the ESNA1-K membrane was more severe than that of the HL membrane.

Two distinct membrane fouling stages were observed with the two membranes, possibly associated with two different fouling mechanisms. The membrane flux decreased quickly during the first 300 min of each membrane filtration experiment. This initial rapid membrane fouling stage was interpreted as being caused by adsorption of organic matter on the membrane surface and pore blocking. In contrast, after the initial rapid membrane-fouling stage, the rate of membrane flux attenuation decreased; compaction and thickening of the cake layer adsorbed on the membrane surface could cause the second membrane-fouling stage.

### 3.2. Characteristics of the membranes after fouling development

The morphologies of the membranes are shown in Fig. 3. There were significant differences between the fouled membranes and the virgin membranes, and fouling layers could be observed on the surfaces of the fouled membranes (Fig. 3(b),(c),(e), and (f)). The formation of fouling layers on the membrane surfaces altered their interfacial properties, and therefore changed the membrane permeate flux.

AFM images of the two virgin membranes (Fig. 3(g) and (h)) showed that the surface of the HL membrane was smoother with lower roughness (5.758 nm) than the ESNA1-K membrane, which had a rougher surface (55.076 nm). In the case of fouling by TH DOM, the ESNA1-K membrane surface roughness was 27.82 nm (Fig. 3(j)); whereas, the surface roughness of the HL membrane was 44.83 nm (Fig. 3(i)), indicating that the ESNA1-K membrane became smoother after DOM filtration; however, the smooth HL membrane became rougher because organic matter adhered to the membrane surface. It has been reported that high-roughness membranes are easily fouled by organics, and low-roughness membranes are less easily contaminated by organics [26]. These observations are consistent with the results of our experiments, in which the ESNA1-K membrane flux declined faster than that of the HL membrane in the presence of DOM (Fig. 2), i.e. the high-roughness ESNA1-K membrane was more severely fouled than the low-roughness HL membrane in the presence of DOM.

FTIR spectra of the membranes were acquired in order to obtain more information on the chemical structures of the membrane foulants, as shown in Fig. 4. The spectra have broad overlapping bands instead of sharp absorption peaks because of the heterogeneity of the organic matter. Both the DOM-fouled membranes displayed strong absorption bands at  $3,430\text{ cm}^{-1}$ , characteristic of hydrogen bonded OH [28]. The absorption bands by hydrogen bonded NH were also observed at  $3,300\text{ cm}^{-1}$ . Relatively high aliphatic  $\text{CH}_2$  absorption bands were seen at  $2,928\text{ cm}^{-1}$ . The peak near  $1,000\text{--}1,120\text{ cm}^{-1}$  is associated with alcoholic C–O absorption. Alcoholic C–O bonds may originate from polysaccharide-like substances [28]. According to Lee et al. [29], the absorption peaks at  $3,300$  and  $1,650\text{--}1,515\text{ cm}^{-1}$  in the FTIR spectra are associated with peptide bonds in proteins, and the characteristic peaks of polysaccharides are observed at  $3,550\text{--}3,200$ ,  $2,925$ , and  $1,260\text{--}1,000\text{ cm}^{-1}$ . Fig. 4(a) and (b) shows the characteristic absorption peaks of the membrane materials. There were characteristic peaks from both proteins and polysaccharides in the FTIR spectra of the membranes

fouled by DOM (Fig. 4(c)–(f)). This result suggested that proteins and polysaccharides in the DOM were deposited on the membranes during NF, i.e. proteins and polysaccharides were both foulants of the NF membranes.

The contact angles variations for the two membranes after DOM fouling were different, as shown in Fig. 5. The contact angle of the HL membrane increased following fouling by DOM, whereas that of the ESNA1-K membrane was slightly reduced. The contact angle is believed to reflect the hydrophobicity of the membrane surface or fouling layer, i.e. a larger membrane contact angle corresponds to greater hydrophobicity of the membrane surface. Thus, after fouling by DOM, the fouling layer adhered to the HL membrane was more hydrophobic than the virgin membrane, whereas there was no obvious change in the hydrophobicity of the ESNA1-K membrane after fouling compared with the virgin membrane. However, both SEM and AFM results showed that the ESNA1-K membrane did intercept DOM and form a fouling layer, leading to membrane fouling. These results indicated that the DOM fouling layer had a different effect on the contact angles of the two membranes. In addition, for the same type of membrane the contact angle changes were similar after filtering different types of DOM (Fig. 5). This result indicates that the hydrophobicity of the membrane surfaces were similar after the adsorption of DOM on the membrane surface, i.e. the hydrophobicities of the organic matter adsorbed on the membrane surfaces tended to be similar.

### 3.3. Characteristics of different types of DOM

The MW distribution is an important characteristic of the organic matter, which not only characterizes the molecular size of the DOM but is also an important factor in membrane fouling [28]. The MW distributions of the DOM before and after NF are shown in Fig. 6. The MW spectra of QCS DOM and TH DOM (Fig. 6(a) and (b), respectively) are similar, using either the TOC detector or the UV detector. Three major peak clusters with MWs of 800 kDa, 2,000, and 800 Da were observed in the feed water (Fig. 6(a) and (b)); DOM with MWs greater than 100 kDa and between 10 and 1 kDa consisted of both hydrophobic and hydrophilic substances, and DOM with MWs between 300 and 1,000 Da mainly contained hydrophilic substances (Fig. 6(c) and (d)).

DOM with MWs greater than 10 kDa showed a low UV response, which indicated that this high-MW portion of the organics contained polysaccharides, proteins or polymer colloids with lower UV

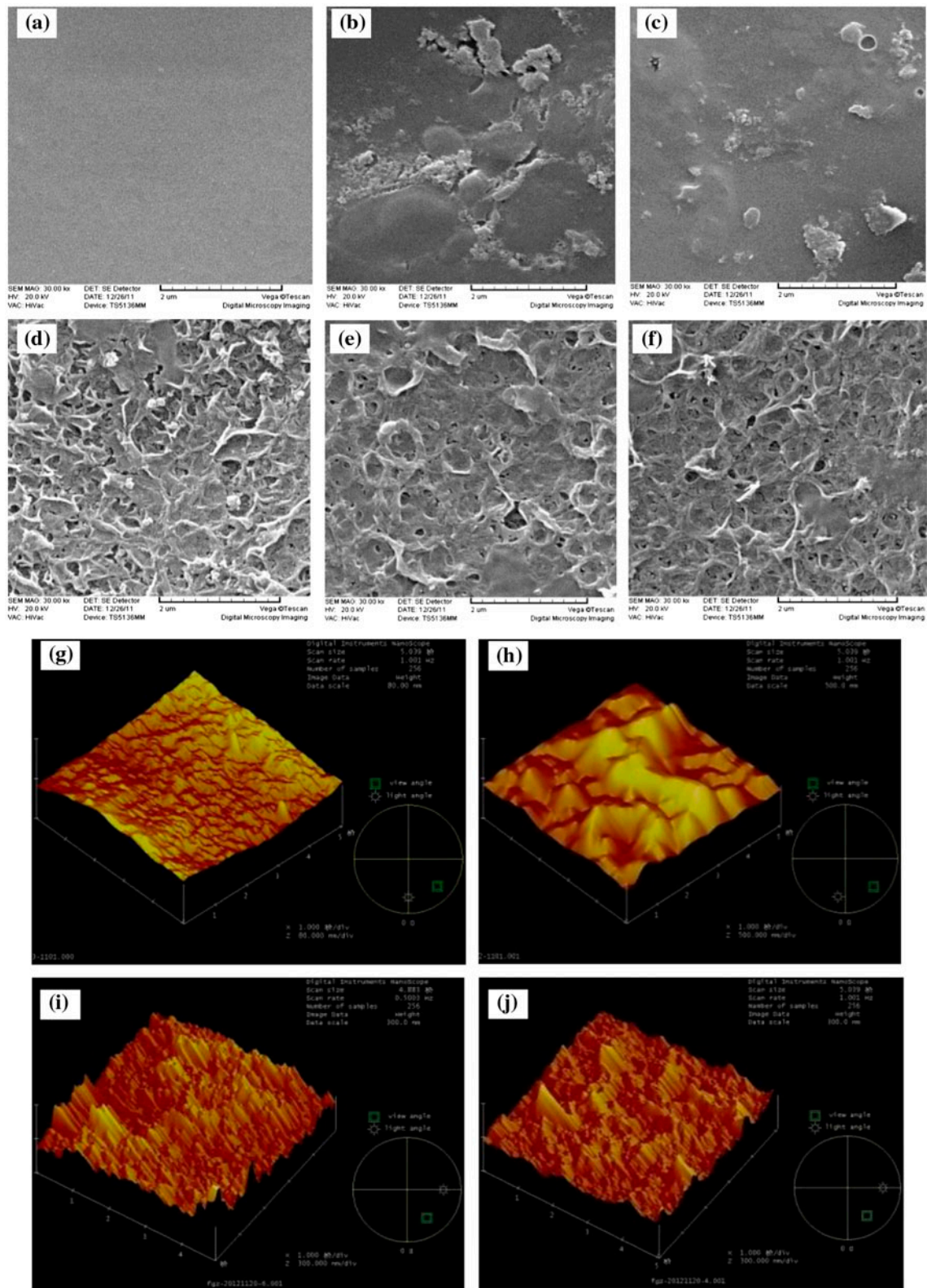


Fig. 3. SEM and AFM images of virgin and fouled membranes in presence of different DOM: (a) HL-virgin membrane; (b) HL-TH DOM; (c) HL-QCS DOM; (d) ES-virgin membrane; (e) ES-TH DOM; (f) ES-QCS DOM; (g) HL-virgin membrane; (h) ES-virgin membrane; (i) HL-TH DOM; (j) ES-TH DOM. Note: The legend “ES” represent the ESNA1-K membrane.

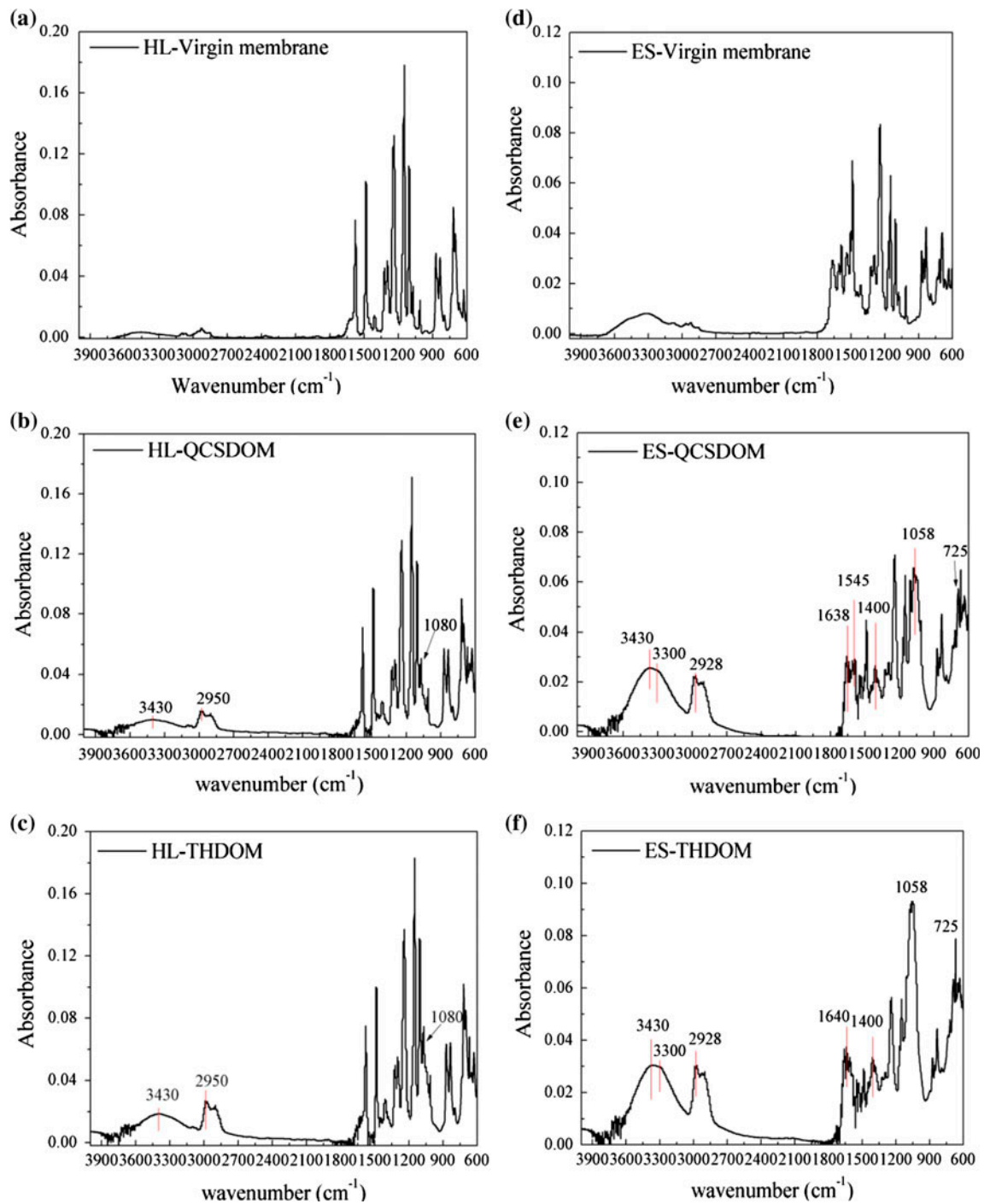


Fig. 4. FTIR spectra of virgin and fouled membranes: (a) HL-virgin membrane; (b) HL-QCS DOM; (c) HL-TH DOM; (d) ES-virgin membrane; (e) ES-QCS DOM; (f) ES-TH DOM. Note: The legend “ES” represent the ESNA1-K membrane.

absorptions. The molecular sizes of this part of the DOM were much larger than the NF membrane pore size; therefore, these molecules were easily intercepted by NF. The high-MW organics in TH DOM had a larger proportion of hydrophobic components (Fig. 6(d))

than QCS DOM; consequently, the interaction force with the membrane surface was lower for the membrane surface with higher hydrophilicity. Therefore, the larger organics did not easily adhere to the membrane surface to form a fouling layer, and were

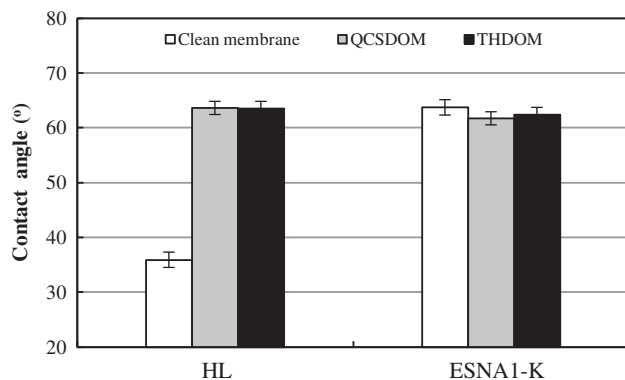


Fig. 5. Contact angle of virgin and fouled membranes after 8 h of NF in the presence of different DOM. Note: The legend “ES” represent the ESNA1-K membrane. Error bar indicates standard deviation of repetitive experiments.

instead loosely attached to the fouling layer formed by smaller molecular organic compounds; nevertheless, this portion of the organic matter played an active role in forming the fouling layer.

Organics of medium-MW, i.e. between 1.5 and 10 kDa, accounted for a small part of the DOM and were partly retained by the NF membranes; these molecules were intercepted by the membrane surface and were important components of the fouling layer. Fig. 6(a) shows that the TOC response for this portion of organics was not high, which indicated that the proportion of the DOM with medium-MW was small. However, this portion of organics showed a strong UV response which indicated that this portion might contain humic-like substances with benzene or  $\pi$ -bonded structures or protein-like organics containing benzene rings with conjugated double-bonds, such as tryptophan and tyrosine. The medium-MW DOM had a larger proportion of hydrophobic components; the two NF membranes had hydrophilic surface characteristics, and therefore, the hydrophobic components of the medium-MW organics did not easily adhere to on the membrane surface, but hydrophilic compounds were easily adsorbed on the membrane surface, causing membrane fouling. The medium-MW organics were partly retained and the portion permeated the NF membranes was mainly hydrophobic humic-like organics.

The membranes showed substantial differences between their respective removal efficiencies for DOMs with MWs lower than 1.5 kDa. The ESNA1-K membrane exhibited higher removal efficiencies compared with the HL membrane. In addition, the UV response of the permeate samples of low-MW DOM was much lower than that of the feed water

(Fig. 6(b)), which suggested that the NF membrane retained much of the hydrophilic DOM in this portion of organics. The low-MW DOM was adsorbed on the membrane surface, forming a fouling layer, or entered into the membrane pores, causing a reduction in MW cut off (MWCO), thereby contributing to the membrane flux attenuation.

Therefore, the DOM with low-MW were able to enter the membrane pores, and the high- and medium-MW DOM were able to adhere to the membrane surfaces, which had obvious influences on NF fouling. The MWCO of the NF membranes were reduced by pore blockage by the low-MW DOM, and the membrane hydrophobicities were changed by the retention of high- and medium-MW DOMs, all of which might have caused flux decline and membrane fouling.

### 3.4. Mechanism of NF membrane fouling by DOM

The cohesion free energy ( $\Delta G_{131}^{CO}$ ) and adhesion free energy ( $\Delta G_{132}^{AD}$ ) between the membrane and foulants were estimated based on the contact angles of three different liquids (Milli-Q water, methylene diiodide, and propanetriol) [30], as shown in Table 4. The cohesion free energy expresses the thermodynamic stability (hydrophobicity) of a substance; a more negative cohesion free energy reflects a weaker stability and a tendency to congregate in water, and thus a greater hydrophobicity [30]. As shown in Table 4, QCS DOM and TH DOM both had negative cohesion free energies; therefore, the two types of DOM exhibited hydrophobic characteristics. The cohesion free energy of TH DOM was more negative than that of QCS DOM, which suggested that the hydrophobicity of TH DOM was greater than that of QCS DOM. This was in agreement with the results of the HPSEC-UV-TOC analyses. Therefore, it could be inferred that the cake layer formed by TH DOM had a denser structure and had a greater effect on flux reduction.

The adhesion free energy describes the interaction forces between foulants and the membrane in the filtration process. A higher negative adhesion free energy indicates that the attraction forces between the foulants and membrane are much stronger, and the foulants are more easily adsorbed in the membrane holes or trapped on the membrane surface, resulting in irreversible membrane fouling [30]. As shown in Table 5, the adhesion free energies between TH DOM and the membranes were both more negative than those between QCS DOM and the membranes, indicating that the interactions between TH DOM and the membranes were much stronger. The TH DOM adhered more easily to the membranes and caused membrane fouling. A comparison of the adhesion free

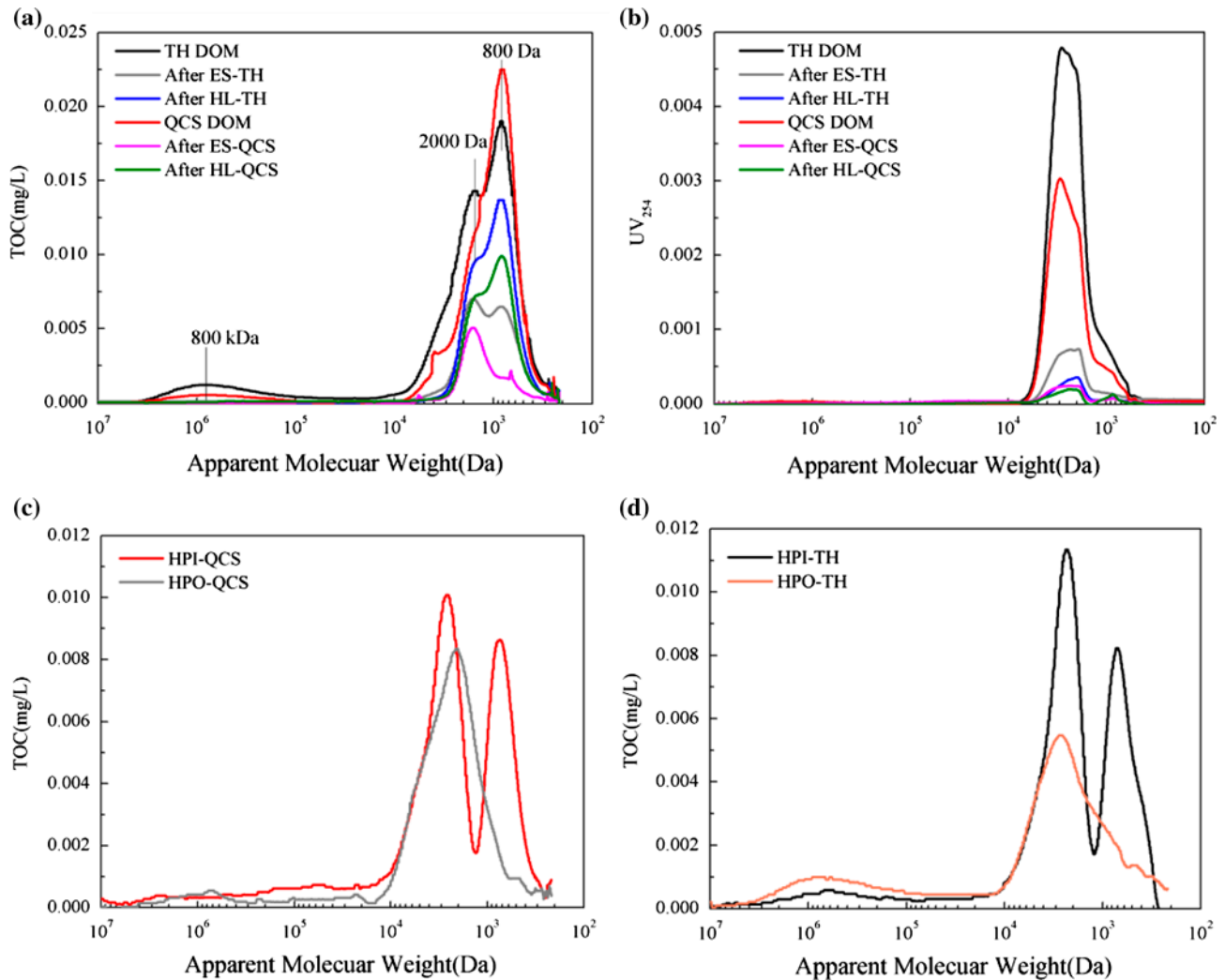


Fig. 6. MW distributions of DOM samples measured by HPSEC with (a) TOC detectors, (b) UV detectors, (c) hydrophobic (HPO) and hydrophilic (HPI) fractions of QCS DOM samples, and (d) hydrophobic (HPO) and hydrophilic (HPI) fractions of TH DOM samples in the feed water.

Note: The legend “ES” represent the ESNA1-K membrane.

Table 4  
Cohesion free energy of membrane and foulants

|             | $\gamma^{lw}$ | $\gamma^{AB}$ | $\gamma^+$ | $\gamma^-$ | $\Delta G_{131}^{LW}$ | $\Delta G_{131}^{AB}$ | $\Delta G_{131}^{CO}$ |
|-------------|---------------|---------------|------------|------------|-----------------------|-----------------------|-----------------------|
| HL membrane | 29.21         | 28.1          | 6.25       | 31.65      | -1.08                 | 5.94                  | 5.89                  |
| ES membrane | 22.08         | 19.96         | 4.7        | 21.19      | -0.002                | -5.14                 | -5.14                 |
| TH DOM      | 35.23         | 9.34          | 1.57       | 13.93      | -3.21                 | -20.01                | -23.22                |
| QCS DOM     | 29.41         | 12            | 2.34       | 15.42      | -1.14                 | -15.82                | -16.96                |

energies between the membranes and the DOM showed that the adhesion free energies between the ESNA1-K membrane and the DOM were higher. It can be concluded that the membrane fouling induced

by DOM was greater for the ESNA1-K membrane than for the HL membrane; this observation agrees well with the flux attenuation observed in the fouling development stage with the two NF membranes.

Table 5  
Adhesion free energy of membrane and foulants

|            | $\Delta G_{132}^{LW}$ | $\Delta G_{132}^{AB}$ | $\Delta G_{132}^{AD}$ |
|------------|-----------------------|-----------------------|-----------------------|
| HL-TH DOM  | -0.638                | -2.317                | -2.954                |
| HL-QCS DOM | -0.269                | -1.646                | -1.915                |
| ES-TH DOM  | -0.965                | -20.622               | -21.587               |
| ES-QCS DOM | -0.367                | -18.386               | -18.753               |

It was previously reported that the adhesion free energy is related to the initial decline of the flux [31]. As shown in Fig. 2, the initial flux of the ESNA1-K membrane declined faster than that of the HL membrane during the filtration of DOM; these results are in good agreement with the results of the adhesion free energy calculations (Table 5). The more negative adhesion free energy between the foulants and the membrane resulted in a faster and larger decline of the membrane flux.

### 3.5. Effect of the fouling layer on removal of NPX by NF membranes

To investigate the effects of membrane fouling on the rejection behavior of NPX, the filtration of a solution containing 100  $\mu\text{g/L}$  of NPX was examined after formation of the fouling layer on the membrane surface. As shown in Fig. 7, the presence of QCS DOM significantly increased the NPX rejection; however, the presence of TH DOM decreased the NPX rejection rate, which indicated that the NPX removal behavior was different for different DOM-fouled membranes. Based on the previous analysis, the different MW distributions, hydrophobic properties of the DOM, and characteristics of the fouling layer adhered to the membrane surface were correlated to the effects on NPX rejection by the NF membranes.

The octanol–water partition coefficient ( $\log K_{OW}$ ) of NPX is 3.18, and NPX is hydrophobic [32]. According to the Hamaker constant (proportionality constant) between membranes and water solutes, the force between hydrophobic solutes and a hydrophobic membrane is larger when there is severe membrane fouling. Therefore, a membrane with a strong hydrophobic surface could adsorb NPX more easily; as a result, higher NPX rejection would be achieved. It is worthwhile to note that under experimental conditions (pH 8.0), NPX is negatively charged ( $\text{pK}_a$  4.2, Table 1). One of the main removal mechanisms for negatively charged NPX is electrostatic repulsion; therefore, it was hypothesized that the altered surface charge on the fouling layer was responsible for the variations in the rejection of NPX. As shown in Table 6, the surface

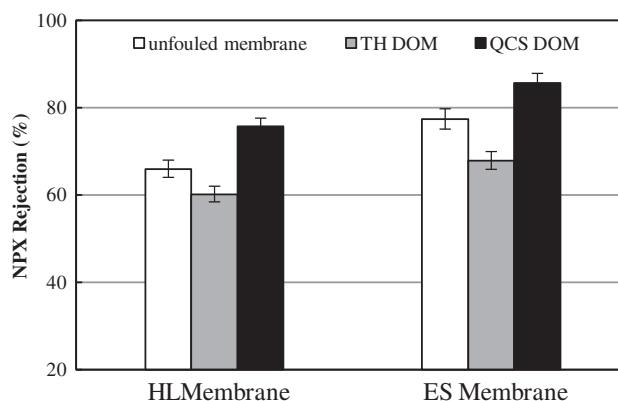


Fig. 7. Rejection of NPX by unfouled and fouled NF membranes.

Note: The legend “ES” represent the ESNA1-K membrane. Error bars shows standard deviation of repetitive experiments.

charge of the DOM-fouled membrane was more negative than that of the virgin for HL membrane, and less negative than that of the virgin for ESNA1-K membrane. In addition, a more negative surface charge was observed for the QCS-DOM-fouled membranes than the TH-DOM-fouled membranes. Therefore, there will be a great extent of electrostatic repulsion between NPX and the QCS-DOM-fouled membranes, while less electrostatic repulsion between NPX and the TH-DOM-fouled membranes.

Surface free energy analysis indicated that both the two DOM had negative cohesion free energies and exhibited hydrophobicity, namely tendency to cohere on the membrane surface. With the higher negative adhesion free energies between DOM foulants and the NF membrane, the attraction forces between them are much stronger; therefore, DOM foulants are more easily adsorbed in the membrane pores and trapped on the membrane surface to form a fouling layer. Consequently, a denser membrane fouling layer with negatively charged and hydrophobicity characteristics formed in the presence of DOM, which was

Table 6  
Surface charge of virgin and DOM fouled membranes

|                    | Zeta potential at pH 8.0 (mv) |
|--------------------|-------------------------------|
| HL-virgin membrane | -27.42                        |
| HL-QCS DOM         | -76.94                        |
| HL-TH DOM          | -56.58                        |
| ES-virgin membrane | -82.44                        |
| ES-QCS DOM         | -81.19                        |
| ES-TH DOM          | -70.97                        |

responsible for the variation of the NPX retention and membrane flux declination.

The formation of the fouling layer could also interfere with the solute-membrane interaction [19]. When a denser fouling layer was formed by DOM deposition during the filtration process, the electrostatic repulsion and hydrophobic adsorption between NPX and the NF membrane changed into the effect between NPX and the membrane fouling layer. The negatively charged NPX can be removed by considerable electrostatic repulsion owing to more negatively charged membrane fouling layer. It can not be denied that hydrophobicity was beneficial to the increased NPX rejection. Hajibabania et al. [33] reported that hydrophobic ionic trace organics adsorbed considerably less due to electrostatic repulsion between the model NOM (Humic and alginate) and the charged trace organics. Therefore, it was hypothesized that the more electrostatic repulsion was the main reason for the increased NPX retention. However, the hydrophobic adsorption could be one of the important factors affecting NPX retention. And membrane pore blockage caused by low-MW DOM contributed to the increased NPX retention, simultaneously. In contrast, the cake-enhanced concentration polarization effect caused by the fouling layer, which led to a lower trace organics rejection as the previous reported [19,34], could be the main reason of the decreased NPX rejection for TH-DOM-fouled membrane in this study. It was the result of more severe membrane fouling in the presence of TH DOM, which reflected by the faster membrane flux declination. In addition, the surface energy analysis described in Section 3.4 also indicated that the fouling layer formed by TH DOM was denser than that of QCS DOM. Therefore, the concentration polarization of the TH DOM fouling layer was more obvious than that of QCS DOM, which increased the amount of NPX across the membrane and lowered the rejection rate. Consequently, the increased NPX rejection was mainly attributed to electrostatic repulsion, whereas the decreased NPX rejection was mainly attributed to cake-enhanced concentration polarization.

Therefore, membrane fouling had a considerable influence on the removal of NPX, resulting in either an increase or decrease in rejection, which can be interpreted as being a function of competing fouling mechanisms.

#### 4. Conclusions

- (1) Membrane fouling caused by natural DOM had a considerable influence on the separation

of NPX, and severe membrane fouling was associated with the adsorption of DOM on the membrane surface and the formation of a fouling layer. Medium- and high-MW DOM were the main components of the fouling layer formed on the membrane surface; low-MW DOM was associated with membrane pore blockage. These factors played important roles in membrane flux decline and the effects on NPX rejection.

- (2) A high-roughness membrane was more easily fouled by DOM, whereas a low-roughness membrane was not that easily contaminated by organics, proteins, and polysaccharides in the DOM, which could be deposited on the membrane surface and were foulants for both NF membranes. A more negative adhesion free energy between foulants and the membrane resulted in a faster membrane flux decline and severe membrane fouling. A more negative cohesion free energy of the organics resulted in the formation of a denser fouling layer on the membrane surface and more severe membrane fouling.
- (3) Membrane fouling by natural DOM resulted in either an increase or decrease in NPX rejection depending on the type of DOM; this result was interpreted as being a function of competing fouling mechanisms. The increased NPX rejection by QCS-DOM-fouled membrane was mainly attributed to electrostatic repulsion, whereas the decreased NPX rejection by TH-DOM-fouled membrane was mainly attributed to cake-enhanced concentration polarization.

#### Acknowledgments

This research was financially supported by the National Water Pollution Control and Treatment Key Technologies R&D Program (Project 2011ZX07410-002-1) and the National Natural Science Foundation of China (Grant no. 51208365).

#### References

- [1] Y. Magara, S. Kunikane, M. Itoh, Advanced membrane technology for application to water treatment, *Water Sci. Technol.* 37 (1998) 91–99.
- [2] W. Ma, Z. Sun, Z. Wang, Y.B. Feng, T.C. Wang, U.S. Chan, C.H. Miu, S. Zhu, Application of membrane technology for drinking water, *Desalination* 119 (1998) 127–131.

- [3] K. Kimura, G. Amy, J.E. Drewes, Y. Watanabe, Adsorption of hydrophobic compounds onto NF/RO membranes: An artifact leading to overestimation of rejection, *J. Membr. Sci.* 221 (2003) 89–101.
- [4] K. Kimura, G. Amy, J. Drewes, T. Heberer, T.U. Kim, Y. Watanabe, Rejection of organic micropollutants (disinfection by-products, endocrine disrupting compounds, and pharmaceutically active compounds) by NF/RO membranes, *J. Membr. Sci.* 227 (2003) 113–121.
- [5] Y. Yoon, P. Westerhoff, J. Yoon, Removal of 17 $\beta$  estradiol and fluoranthene by nanofiltration and ultrafiltration, *J. Environ. Eng.* 130 (2004) 1460–1467.
- [6] Y. Yoon, P. Westerhoff, S.A. Snyder, E.C. Wert, Nanofiltration and ultrafiltration of endocrine disrupting compounds, pharmaceuticals and personal care products, *J. Membr. Sci.* 270 (2006) 88–100.
- [7] A.I. Schäfer, A.G. Fane, T.D. Waite, Fouling effects on rejection in the membrane filtration of natural waters, *Desalination* 131 (2000) 215–224.
- [8] D. Violleau, H. Essis-Tome, H. Habarou, J.P. Croué, M. Pontié, Fouling studies of a polyamide nanofiltration membrane by selected natural organic matter: An analytical approach, *Desalination* 173 (2005) 223–238.
- [9] N.H. Lee, G. Amy, J.P. Croue, H. Buisson, Morphological analyses of natural organic matter (NOM) fouling of low-pressure membranes (MF/UF), *J. Membr. Sci.* 261 (2005) 7–16.
- [10] Y. Kaiya, Y. Itoh, K. Fujita, S. Takizawa, Study on fouling materials in the membrane treatment process for potable water, *Desalination* 106 (1996) 71–77.
- [11] G. Amy, Fundamental understanding of organic matter fouling of membranes, *Desalination* 231 (2008) 44–51.
- [12] H. Huang, N. Lee, T. Young, A. Gary, J.C. Lozier, J.G. Jacangelo, Natural organic matter fouling of low-pressure, hollow-fiber membranes: Effects of NOM source and hydrodynamic conditions, *Water Res.* 41 (2007) 3823–3832.
- [13] A.W. Zularisam, A.F. Ismail, R. Salim, Behaviours of natural organic matter in membrane filtration for surface water treatment—A review, *Desalination* 194 (2006) 211–231.
- [14] J.A. Leenheer, J.P. Croué, Peer reviewed: Characterizing aquatic dissolved organic matter, *Environ. Sci. Technol.* 37 (2003) 18A–26A.
- [15] E.C. Devitt, M.R. Wiesner, Dialysis investigations of atrazine–organic matter interactions and the role of a divalent metal, *Environ. Sci. Technol.* 32 (1998) 232–237.
- [16] N.A. Kulikova, I.V. Perminova, Binding of atrazine to humic substances from soil, peat and coal related to their structure, *Environ. Sci. Technol.* 36 (2002) 3720–3724.
- [17] H. Yamamoto, H.M. Liljestrand, Y. Shimizu, M. Morita, Effects of physical–chemical characteristics on the sorption of selected endocrine disruptors by dissolved organic matter surrogates, *Environ. Sci. Technol.* 37 (2003) 2646–2657.
- [18] D.M. Annalisa, A.J.C. Semiao, A.L. Blanca, Retention of pesticide Endosulfan by nanofiltration: Influence of organic matter–pesticide complexation and solute–membrane interactions, *Water Res.* 47 (2013) 3484–3496.
- [19] L.D. Nghiem, D. Vogel, S. Khan, Characterising humic acid fouling of nanofiltration membranes using bisphenol A as a molecular indicator, *Water Res.* 42 (2008) 4049–4058.
- [20] L.D. Nghiem, P.J. Coleman, C. Espendiller, Mechanisms underlying the effects of membrane fouling on the nanofiltration of trace organic contaminants, *Desalination* 250 (2010) 682–687.
- [21] M. Carballa, F. Omil, J.M. Lema, M. Llopart, C. García-Jares, I. Rodríguez, M. Gómez, T. Ternes, Behavior of pharmaceuticals, cosmetics and hormones in a sewage treatment plant, *Water Res.* 38 (2004) 2918–2926.
- [22] K. Xia, A. Bhandari, K. Das, G. Pillar, Occurrence and fate of pharmaceuticals and personal care products (PPCPs) in biosolids, *J. Environ. Qual.* 34 (2005) 91–104.
- [23] G.R. Boyd, H. Reemtsma, D.A. Grimm, S. Mitra, Pharmaceuticals and personal care products (PPCPs) in surface and treated waters of Louisiana, USA and Ontario, Canada, *Sci. Total Environ.* 311 (2003) 135–149.
- [24] L.D. Nghiem, A.I. Schäfer, M. Elimelech, Pharmaceuticals retention mechanisms by nanofiltration membranes, *Environ. Sci. Technol.* 39 (2005) 7698–7705.
- [25] S. Wong, J.V. Hanna, S. King, T.J. Carroll, R.J. Eldridge, D.R. Dixon, B.A. Bolto, S. Hesse, G.A.-B. Hesse, F.H. Frimmel, Fractionation of natural organic matter in drinking water and characterization by <sup>13</sup>C cross-polarization magic-angle spinning NMR spectroscopy and size exclusion chromatography, *Environ. Sci. Technol.* 36 (2002) 3497–3503.
- [26] N. Park, B. Kwon, I.S. Kim, Biofouling potential of various NF membranes with respect to bacteria and their soluble microbial products (SMP): Characterizations, flux decline, and transport parameters, *J. Membr. Sci.* 258 (2005) 43–54.
- [27] Z. Liu, Research on the identification of main membrane foulants and relative characterization method, Tongji University, Shanghai, 2010.
- [28] N. Her, G. Amy, H.-R. Park, M. Song, Characterizing algogenic organic matter (AOM) and evaluating associated NF membrane fouling, *Water Res.* 38 (2004) 1427–1438.
- [29] N. Lee, G. Amy, J.P. Croué, Low-pressure membrane (MF/UF) fouling associated with allochthonous versus autochthonous natural organic matter, *Water Res.* 40 (2006) 2357–2368.
- [30] C.J. van Oss, Chapter two the apolar and polar properties of liquid water and other condensed-phase materials, *Interface Sci. Technol.* 16 (2008) 13–30.
- [31] Q. Li, M. Elimelech, Organic fouling and chemical cleaning of nanofiltration membranes: Measurements and mechanisms, *Environ. Sci. Technol.* 38 (2004) 4683–4693.
- [32] V. Yangali-Quintanilla, A. Sadmani, M. McConville, M. Kennedy, G. Amy, Rejection of pharmaceutically active compounds and endocrine disrupting compounds by clean and fouled nanofiltration membranes, *Water Res.* 43 (2009) 2349–2362.
- [33] S. Hajibabania, A. Verliefe, J.A. McDonald, S.J. Khan, P. Le Clech, Fate of trace organic compounds during treatment by nanofiltration, *J. Membr. Sci.* 373 (2001) 130–139.
- [34] L.D. Nghiem, A.I. Schäfer, M. Elimelech, Removal of natural hormones by nanofiltration membranes: Measurement, modeling, and mechanisms, *Environ. Sci. Technol.* 38 (2004) 1888–1896.